frontiers | Frontiers in Oncology

TYPE Original Research
PUBLISHED 29 August 2025
DOI 10.3389/fonc.2025.1628054



OPEN ACCESS

EDITED BY
Maria Chiara Zatelli,
University of Ferrara, Italy

REVIEWED BY
Hailin Tang,
Sun Yat-sen University Cancer Center (SYSUCC), China
Zheng Yuan,
China Academy of Chinese Medical Sciences, China

*CORRESPONDENCE
Fei Yin
47100214@hebmu.edu.cn

RECEIVED 13 May 2025
ACCEPTED 11 August 2025
PUBLISHED 29 August 2025

CITATION
Feng M, Zhao M, Duan X, Hou J, Wang Q and Yin F (2025) Visualized clinical–radiomics model for predicting the efficacy of surufatinib in hepatic metastases of neuroendocrine neoplasms.
*Front. Oncol.* 15:1628054.
doi: 10.3389/fonc.2025.1628054



# Visualized clinical–radiomics model for predicting the efficacy of surufatinib in hepatic metastases of neuroendocrine neoplasms

Miaomiao Feng[1], Man Zhao[1], Xiaoling Duan[1], Jiaojiao Hou[1], Qi Wang[2] and Fei Yin[1]*

[1]Department of Gastroenterology, Fourth Hospital of Hebei Medical University, Shijiazhuang, Hebei, China, [2]Department of CT and MRI, Fourth Hospital of Hebei Medical University, Shijiazhuang, Hebei, China

**Background:** Hepatic metastatic neuroendocrine neoplasms (HM-NENs) have few treatment biomarkers and low survival rates. We created a clinical–radiomics fusion model to predict surufatinib efficacy in HM-NENs and presented it as a nomogram, meeting unmet requirements in precision hepatology.
**Methods:** This study included 76 HM-NEN patients (131 hepatic metastases) treated with surufatinib. SlicerRadiomics was used to extract radiomics features from arterial phase computed tomography (APCT). The least absolute shrinkage and selection operator (LASSO) was used to select radiomics features and calculate a radiomics score (Radscore). Multivariable logistic regression analysis was utilized to create the clinical–radiomics fusion model, which included clinical characteristics and Radscore and was displayed as a nomogram. The area under the receiver operating characteristic curve (ROC) was used to assess model performance, and internal validation was done using the bootstrap resampling approach.
**Results:** After multivariate logistic regression analysis, the Radscore, Ki67 antigen (Ki67), number of hepatic metastases, and extrahepatic metastasis were included as predictors in the final model. The area under the curve (AUC) of the clinical–radiomics fusion model to predict the response of surufatinib of HM-NENs was 0.928 (95% CI: 0.885 - 0.971). The AUC verified by bootstrap is 0.928 (95% CI: 0.881–0.965), indicating a good performance of the fusion model.
**Conclusion:** The clinical–radiomics fusion model can effectively identify patients with HM-NENs sensitive to surufatinib therapy. The nomogram provided clinicians with a convenient and dependable tool for decision-making.

KEYWORDS

**hepatic metastatic neuroendocrine neoplasms, surufatinib, clinical-radiomics model, arterial phase computed tomography, efficacy**

# 1 Introduction

Neuroendocrine neoplasms (NENs) are a varied group of cancers that originate from the diffuse neuroendocrine systems (1). NENs can occur anywhere in the body, with lung and gastrointestinal pancreatic NENs being the most common (2, 3). The diagnostic capabilities for NENs have improved over time due to advancements in endoscopic techniques and biomarker technologies. The incidence rate has increased sixfold in the last 40 years (4). At present, the primary treatment modalities for NENs encompass surgical resection, chemotherapy, radiotherapy, and immunotherapy. Beyond these, targeted therapy also serves as a therapeutic option. NENs, characterized by abundant vascular supply, dense capillary networks, and elevated vascular endothelial growth factor (VEGF) expression, present opportunities for anti-angiogenic therapy (5).

Surufatinib, an oral tyrosine kinase inhibitor (TKI) developed in China, targets the VEGF receptor (VEGFR), fibroblast growth factor receptor 1 (FGFR1), and colony-stimulating factor 1 receptor (CSF1R), achieving synergistic antitumor activity through both anti-angiogenic and immunomodulatory effects (6). Surufatinib was approved in China in December 2020 and June 2021 for extra-pancreatic and pancreatic NENs, respectively, based on the SANEN-ep and SANEN-p studies (7, 8). Consequently, surufatinib became China's first novel NEN-targeted medication and the first TKI worldwide to treat all NEN subtypes. Previous research has shown that NENs have a relative tendency for the liver, regardless of initial location, with approximately 82% of NEN patients developing hepatic metastases during the course of their illness (9, 10). Patients with HM-NENs experienced a 6.1-fold higher risk of mortality than those without metastases, with their 5-year overall survival rate ranging from 13% to 54%. The 5-year survival rate for pancreatic HM-NENs was 13%–54% compared with 75%–99% in the absence of metastasis (11, 12). Therefore, identifying patients who are sensitive to surufatinib is of crucial importance. In this study, a novel radiomics-based approach is proposed to address this need.

How to quickly and non-invasively screen patients who are sensitive to surufatinib is an urgent problem to be solved. APCT was widely utilized for tumor diagnosis and therapy assessment, and it helped identify optimal candidates via pretreatment imaging (13–15). Radiomics, an emerging technology quantifying tumor heterogeneity via imaging features, has shown promise in oncology prognosis (16). Previous studies have shown that radiomics models of liver MRI can help predict the chronicity of drug-induced liver injury (17). This study integrates radiomics features and clinical characteristics to develop a fusion model for predicting the short-term efficacy of surufatinib in HM-NENS, providing clinicians with an accurate, practical, and visible prediction tool.

**Abbreviations:** HM-NENs, hepatic metastatic neuroendocrine neoplasms; Ki67, Ki67 antigen; NSE, neuron-specific enolase; Mrecist, Modified Response Evaluation Criteria In Solid Tumors; ROC, receiver operating characteristic curve; AUC, area under the curve; DCA, decision curve analysis; LASSO, least absolute shrinkage and selection operator; NPV, negative predictive value; PPV, positive predictive value; Radscore, radiomics score; APCT, arterial phase computed tomography; ROI, region of interest; CR, complete response; PR, partial response; SD, stable disease; PD, progressive disease; VOI, volume of interest

# 2 Materials and methods

## 2.1 Patients

This retrospective study was approved by the Research Ethical Committee of The Fourth Hospital of Hebei Medical University. We evaluated the medical data of HM-NEN patients treated with surufatinib at the Fourth Hospital of Hebei Medical University from January 2018 to December 2024.

Patients were included if (1) age ≥18 years with histopathologically confirmed NENs, (2) received surufatinib therapy, (3) hepatic metastases with ≥1 measurable lesion at baseline, (4) expected survival ≥3 months, and (5) availability of APCT within 1 month before treatment.

Patients were excluded if (1) local therapies were administered during follow-up, (2) concurrent malignancies other than NENs, and (3) poor image quality or incomplete clinical data. The patient selection process was shown in Figure 1. We included a total of 131 hepatic metastatic lesions in 76 patients with HM-NENs. Of these 76 patients, 16 were effective and 60 were ineffective for treatment with surufatinib.

We conducted a clinical follow-up 3 months after administering surufatinib. mRECIST was a modified response criteria for solid tumors. It was especially well suited to assessing targeted treatment for hepatic metastases by concentrating on changes in arterial phase imaging (18). In this study, we used the mRECIST assessment criteria to determine the efficacy of target lesions of hepatic metastases in patients. The following categories were included: (1) complete response (CR): absence of all target lesions, (2) partial response (PR): at least 30% reduction in the total diameters of target lesions, using the baseline sum diameters as a reference, (3) stable disease (SD): there is not enough shrinking to qualify for PR or enough rise to qualify for PD, and (4) progressive disease (PD): At least 20% rise in the total of the diameters of target lesions, based on the smallest sum on examination, or the appearance of one or more additional lesions. Patients' responses to surufatinib were divided into two groups: effective (CR + PR) and ineffective (SD + PD).

## 2.2 Clinical characteristics

Demographic characteristics, Ki67, grade, neuron-specific enolase (NSE), gamma-glutamyl transferase (GGT), alpha-fetoprotein (AFP), the diameter of hepatic metastasis, therapy method, surgery, number of hepatic metastases, extrahepatic metastasis, and tumor location were analyzed.

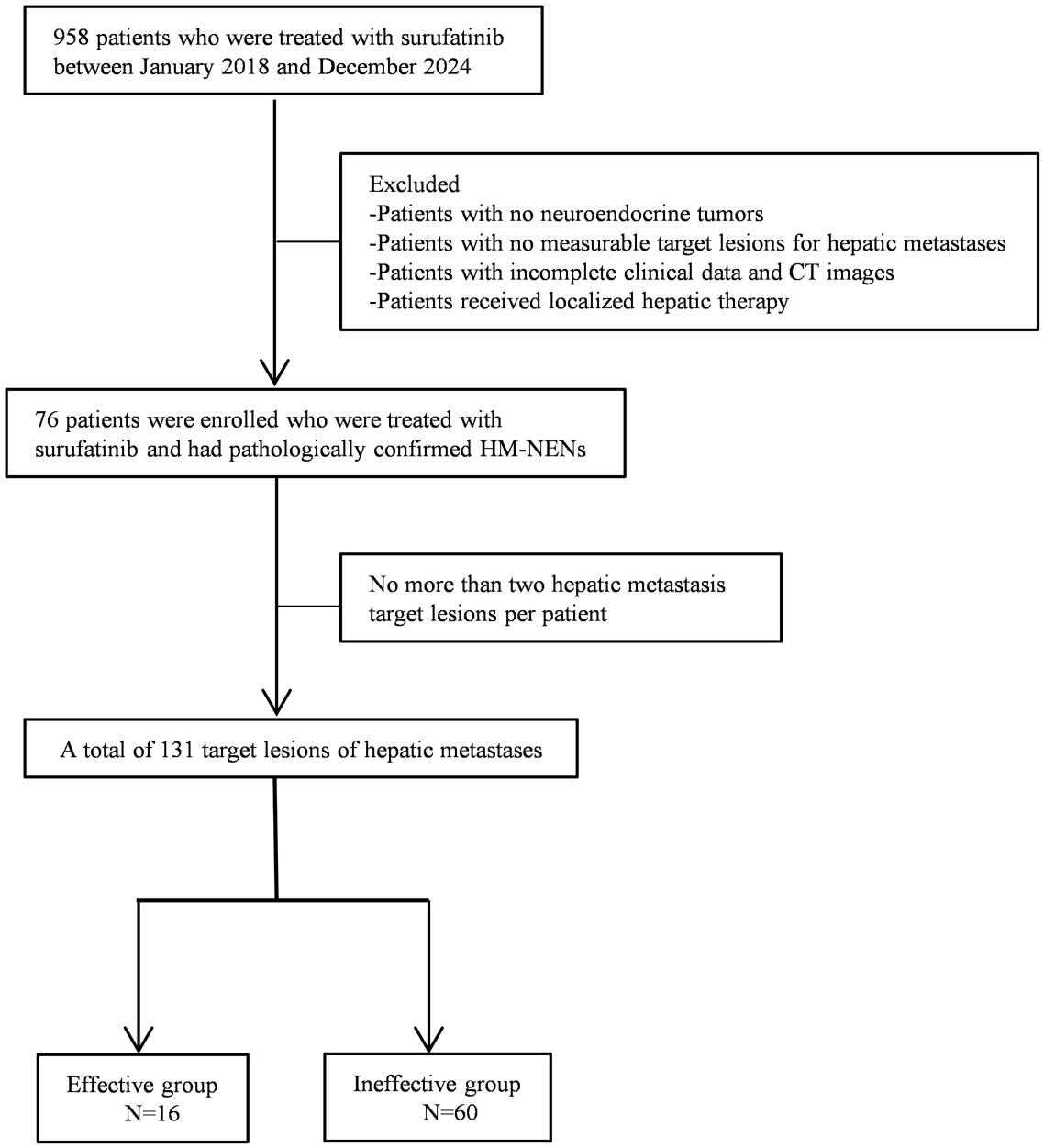


FIGURE 1
Flowchart of this study.

## 2.3 Image segmentation

APCT imaging was conducted using the scan (IQon Spectral CT, Philips Healthcare, Amsterdam, Netherlands), a 256-slice CT system, with the following parameters: tube voltage of 120 kVp, automatic tube current modulation, slice thickness of 5.0 mm, reconstruction increment of 5.0 mm, gantry rotation time of 0.5 s, pitch factor of 0.973, and a standard reconstruction algorithm with a reconstruction section thickness of 1 mm. The APCT images were imported into the 3D Slicer 5.6.2 software (https://www.slicer.org/) in DICOM format. All images were resampled to the same size of $1 \times 1 \times 1$ mm$^3$ and denoised using wavelet filtering. The region of interest (ROI) was manually designated by two clinicians with over 10 years of clinical experience, who were uninformed of the clinicopathological variables and prognosis of the patients. When differences of opinion arose during the drawing process, these were resolved via mutual negotiation. The largest diameter of the hepatic metastases (>1 cm measurable lesion) was selected, and the volume of interest (VOI) was manually drawn layer by layer along the tumor's edge. A maximum of two hepatic metastases were chosen as target lesions per patient. To evaluate the intra- and inter-observer repeatability of ROI segmentation, 46 randomly selected hepatic metastases were re-segmented by the same observer (observer 1) twice at 2-week intervals. Simultaneously, the 46 randomly selected hepatic

metastases were segmented by another observer (observer 2) to evaluate inter-observer repeatability.

## 2.4 Feature extraction and model construction

3D image texture features were extracted from 131 hepatic metastases using the SlicerRadiomics plugin (https://github.com/AIM-Harvard/SlicerRadiomics) in 3D Slicer 5.6.2. The Z-score method was used to standardize the radiomics features. We used intra- and inter-group correlation coefficients (ICC) to evaluate feature extraction repeatability between observers. Radiomic features with ICC <0.75 were excluded. Spearman correlation analysis was used to remove strongly correlated radiomics features, removing those with correlations larger than 0.90. Tenfold cross-validation was performed to determine the hyperparameters in LASSO (19). Finally, a Radscore was calculated by linearly combining the selected features. For the clinical characteristics, multivariate analysis using a backward stepwise selection method was executed via logistic regression to identify independent predictors of efficacy with $p$ <0.05. The Radscore was integrated with clinical characteristics to construct a fusion model. We calculated the AUC, sensitivity, and specificity of the model to evaluate the performance of the model. Internal validation of the model was conducted using bootstrap with 1,000 iterations. The bootstrap approach is crucial in our small-sample studies as it does not need to rely on large-sample assumptions and generates pseudo-samples through resampling to reconstruct the statistical distributions, thus enabling a robust estimation of uncertainty (20). The mean values obtained from these 1,000 resampling procedures were used to evaluate the model's performance. It ensured a complete evaluation of the model's generalization capacity as well as a realistic estimation of its discriminatory power over multiple data subsets typical of the underlying population.

## 2.5 Statistical analyses

The statistical analysis was conducted using R 4.4.2 (https://cran.r-project.org/). Continuous data with a normal distribution were reported as mean ± standard deviation (SD). Continuous data that did not follow a normal distribution were reported as median (upper and lower quartiles). Categorical data were represented using frequencies and percentages. Chi-square test was used to compare categorical variables. Mann–Whitney $U$-test was used to compare continuous variables that did not conform to a normal distribution. For variables with $p$ <0.05 in the univariate analysis, we performed a multivariate logistic regression using backward stepwise selection based on the Wald statistic. Correlation analysis was conducted using Spearman correlation. Calibration curves were plotted to assess the fit of the model. Decision curve analysis (DCA) was used to quantify the NEN benefit under different threshold probabilities and to assess the clinical utility of the model. A $p$-value <0.05 was considered statistically significant.

# 3 Results

## 3.1 Patients' characteristics

A total of 76 patients with 126 hepatic metastases were eligible for inclusion in this study. The mean age was 62 years, and 48.68% of the patients were male. According to mRECIST, the therapeutic effect of surufatinib was CR/PR in 16 (21.05%) patients and SD/PD in 60 (78.95%) patients. The patients' characteristics are shown in Table 1.

In the 76 patients eligible for this study, there were 131 target hepatic metastases. There were no significant differences in AFP, GGT, and surgery between the effective group (CR + PR) and the ineffective group (SD + PD). The other baseline characteristics, including the diameter of the hepatic metastasis, number of hepatic metastases, extrahepatic metastasis, tumor location, NSE, Ki67, grade, and Radscore, were substantially different between the two groups (Table 2).

## 3.2 Feature extraction and radiomics signature building

A total of 851 radiomics features were extracted for each lesion. Among them, there were 14 shape features, 18 first-order features, 24 gray-level co-occurrence matrix (GLCM) features, 16 gray-level size zone matrix (GLSZM) features, 16 gray-level run length matrix (GLRLM) features, five neighboring gray tone difference matrix (NGTDM) features, 14 gray-level dependence matrix (GLDM) features, and 744 wavelet features. Features with ICC of less than 0.75 were excluded, and Spearman correlation analysis was used to remove duplicate features with correlation coefficients larger than 0.90 with other features. After analysis, 60 radiomics features were selected, as shown in Supplementary Table S1. The best radiomics features closely related to efficacy were selected by using LASSO with 10-fold cross-validation. Original_RootMeanSquared, Original_Correlation, Original_LongRunLowGrayLevelEmphasis, Original_Busyness, Wavelet_LLH_Median, Wavelet_LLH_ClusterShade, Wavelet_LLH_Imc1, WaveletH_LLHH_RunVariance, and Wavelet_LLH_SizeZoneNonUniformityNormalized were the optimal radiomics features. Supplementary Figure S1 shows the procedure of LASSO screening. The calculation formula of Radscore is shown below.

10.3389/fonc.2025.1628054

TABLE 1 Patients' characteristics.

| Variable | (Total) *N* = 76 |
|---|---|
| Age[a] | 61.88 ± 11.15 |
| **Sex** | |
| Male | 37 (48.68) |
| Female | 39 (51.32) |
| **NSE** | |
| ≤100 | 15 (19.74) |
| >100 | 61 (80.26) |
| Ki67 [median (IQR)] | 27.50 [7.50, 80.00] |
| AFP, ng/mL [median (IQR)] | 4.60 [2.72, 10.20] |
| GGT, U/L [median (IQR)] | 28.75 [18.45, 53.22] |
| **Grade** | |
| 1 | 7 (9.21) |
| 2 | 29 (38.16) |
| 3 | 8 (10.53) |
| 4 | 32 (42.11) |
| **Number of hepatic metastases** | |
| Oligometastasis | 29 (38.16) |
| Multiple metastases | 36 (47.37) |
| Diffuse metastasis | 11 (14.47) |
| **Diameter of the hepatic metastasis** | |
| 1–3 cm | 52 (68.42) |
| 3–5 cm | 21 (27.63) |
| >5 cm | 3 (3.95) |
| **Tumor location** | |
| EP-NEN | 47 (61.84) |
| PNEN | 29 (38.16) |
| **Extrahepatic metastasis** | |
| No | 43 (56.58) |
| Yes | 33 (43.42) |
| Surgery | |
| No | 52 (68.42) |
| Yes | 24 (31.58) |
| **Therapy method** | |
| Surufatinib + octreotide + chemotherapy and/or immunotherapy | 8 (10.53) |
| Surufatinib + octreotide | 18 (23.68) |
| Surufatinib + chemotherapy and/or immunotherapy | 36 (47.37) |
| Surufatinib | 14 (18.42) |
| **Response** | |
| CR + PR | 16 (21.05) |
| SD + PD | 60 (78.95) |

Unless otherwise indicated, the data are numbers of patients, with percentage in parentheses. NSE, neuron-specific enolase; Ki67, Ki67 antigen; AFP, alpha-fetoprotein; GGT, gamma-glutamyl transferase; EP-NEN, extra-pancreatic neuroendocrine neoplasms; P-NEN, pancreatic neuroendocrine neoplasms.
[a]Data are means ± standard deviation.

$$Radscore = -0.429 \times Original\_RootMeanSquared + 1.054 \times Original\_Correlation + 0.023 \times Original\_LongRunLowGrayLevelEmphasis + 0.406 \times Original\_Busyness - 0.162 \times Wavelet\_LLH\_Median + 0.118 \times Wavelet\_LLH\_ClusterShade + 0.960 \times Wavelet\_LLH\_Imc1 - 0.948 \times WaveletH\_LLHH\_RunVariance + 0.308 \times Wavelet\_LLH\_SizeZoneNonUniformityNormalized$$

Radscore was significantly associated with the response of HM-NENs to surufatinib ($p$ = 0.000), with an AUC of 0.852 (95% confidence interval [CI],0.767–0.922) (Figure 2B).

## 3.3 Development of visualized predictive models

In univariate and multivariate logistic regression analysis (Table 3), Radscore ($p$ = 0.000), Ki67 ($p$ = 0.005), the number of hepatic metastases ($p$ = 0.050), and extrahepatic metastasis ($p$ = 0.009) were identified as independent clinical risk variables. A fusion model that incorporated the independent predictors was developed. The fusion model was displayed as a nomogram, providing clinicians with an effective tool for identifying HM-NEN patients who were susceptible to surufatinib treatment (Figure 3). The AUC of the fusion model was 0.928 (95% CI: 0.885–0.971). The AUC verified by bootstrap is 0.928 (95% CI: 0.881–0.965) (Figure 2). Figure 4A shows the calibration curve of the fusion model. The ideal curve aligned with the calibration prediction curve, validating the superior goodness-of-fit of the fusion model. The decision curve of analysis (DCA) is shown in Figure 4B, where the horizontal axis represents the risk threshold probability, and the vertical direction represents the normalized NEN benefit. DCA indicated that the fusion model provided a greater NEN clinical benefit at the appropriate risk thresholds.

# 4 Discussion

There were individual differences in the responses of patients with HM-NENs to treatment with surufatinib. In our study, more

TABLE 2 Baseline characteristics of effective and ineffective groups in the HM-NENs.

| Variable | Effective group (*n* = 27) | Ineffective group (*n* = 104) | *p* |
|---|---|---|---|
| NSE | | | 0.010 |
| ≤100 | 10 (37.04) | 14 (13.46) | |
| >100 | 17 (62.96) | 90 (86.54) | |
| Ki67 [median (IQR)] | 15.00 [5.00, 30.00] | 30.00 [7.25, 80.00] | 0.050 |
| Grade | | | 0.010 |
| 1 | 3 (11.11) | 10 (9.62) | |
| 2 | 16 (59.26) | 36 (34.62) | |
| 3 | 4 (14.81) | 9 (8.65) | |
| 4 | 4 (14.81) | 49 (47.12) | |
| Tumor location | | | 0.035 |
| EP-NEN | 11 (40.74) | 68 (65.38) | |
| PNEN | 16 (59.26) | 36 (34.62) | |
| Diameter of the hepatic metastasis | | | 0.016 |
| 1–3 cm | 24 (88.89) | 62 (59.62) | |
| 3–5 cm | 3 (11.11) | 35 (33.65) | |
| >5 cm | 0 (0.00) | 7 (6.73) | |
| Number of hepatic metastases | | | 0.018 |
| Oligometastasis | 12 (44.44) | 35 (33.65) | |
| Multiple metastases | 15 (55.56) | 48 (46.15) | |
| Diffuse metastasis | 0 (0.00) | 21 (20.19) | |
| Extrahepatic metastasis | | | 0.002 |
| No | 23 (85.19) | 52 (50.00) | |
| Yes | 4 (14.81) | 52 (50.00) | |
| Surgery | | | 0.531 |
| No | 20 (74.07) | 68 (65.38) | |
| Yes | 7 (25.93) | 36 (34.62) | |
| AFP, ng/mL [median (IQR)] | 3.88 [2.82, 5.90] | 5.32 [2.72, 12.07] | 0.182 |
| GGT, U/L [median (IQR)] | 24.30 [18.90, 44.65] | 33.95 [19.10, 67.97] | 0.152 |
| Radscore [median (IQR)] | 0.78 [0.38, 1.15] | 1.81 [1.25, 2.38] | <0.001 |

Unless otherwise indicated, the data are numbers of patients, with percentage in parentheses. HM-NENs, hepatic metastatic neuroendocrine neoplasms; NSE, neuron-specific enolase; Ki67, Ki67 antigen; AFP, alpha-fetoprotein; GGT, gamma-glutamyl transferase; EP-NEN, extra-pancreatic neuroendocrine neoplasms; P-NEN, pancreatic neuroendocrine neoplasms.

than half of the patients were ineffective on surufatinib (60 out of 76 patients). Therefore, it was necessary to construct an efficient, simple, and visualized prediction tool for clinicians to predict in advance how patients will benefit from the drug and reduce their financial burden. Radiomics, as a novel technology, has the potential to serve as a quantitative decision support tool, and its integration with clinically relevant information could greatly improve clinical prediction capabilities (21, 22). In this study, a clinical–radiomics fusion model was developed and illustrated by a nomogram. The AUC of the fusion model was validated within bootstrap as 0.928 (95% CI: 0.881 - 0.965), demonstrating good predictive performance. Clinicians using this nomogram could efficiently identify patients with HM-NENs who would benefit from surufatinib.

So far, there have been almost no studies on the therapeutic efficacy of surufatinib in HM-NENs. In our study, we developed a personalized visualization combination model that predicted the therapeutic response of hepatic metastases to surufatinib based on the patient's pre-dose APCT. Our study aligned with Lambin's "radiomics signature" concept, where multidimensional data integration enabled a more comprehensive assessment of tumor treatment response (23). Poor therapy response was predicted by elevated Radscore and Ki67 as well as more hepatic and extrahepatic metastases.

While tumor diameter was not an independent predictor of surufatinib efficacy in our study, other HM-NEN prognostic studies highlight the value of quantitative tumor load assessments. One study analyzed the value of quantitative tumor load analysis on baseline MRI in predicting survival in patients with HM-NENs receiving intra-arterial therapy and found that tumor load was a strong independent prognostic factor for overall survival (24, 25). Tumor load was determined by a combination of tumor diameter and the number of tumors; however, our research revealed that tumor diameter was not an independent predictor of surufatinib efficacy. This was attributed to the small percentage of patients in our study who had tumor diameters larger than 5 cm, which totaled only three (3.95%). Previous studies have shown that larger hepatic metastases (>5 cm) exhibited hypoxic microenvironments with lower drug penetration, which was associated with worse responses to targeted therapies (26, 27). The number of hepatic metastases as an independent predictor also reflected tumor load in one way. In deeper subsequent studies, as Zhang et al. demonstrated, circLIFR-007 exerts inhibitory effects on the proliferation and metastasis of breast cancer cells both *in vivo* and *in vitro* (28). As Zeng et al. demonstrated, circMYBL2 promoted the tumorigenesis and aggressiveness of breast cancer (29). Along this line, we can also explore the molecular mechanisms associated with HM-NENs, which may provide a novel targeted therapy for patients with HM-NENs.

Our study does have some limitations: (1) a retrospective single-center design with a small sample size necessitates testing in multi-

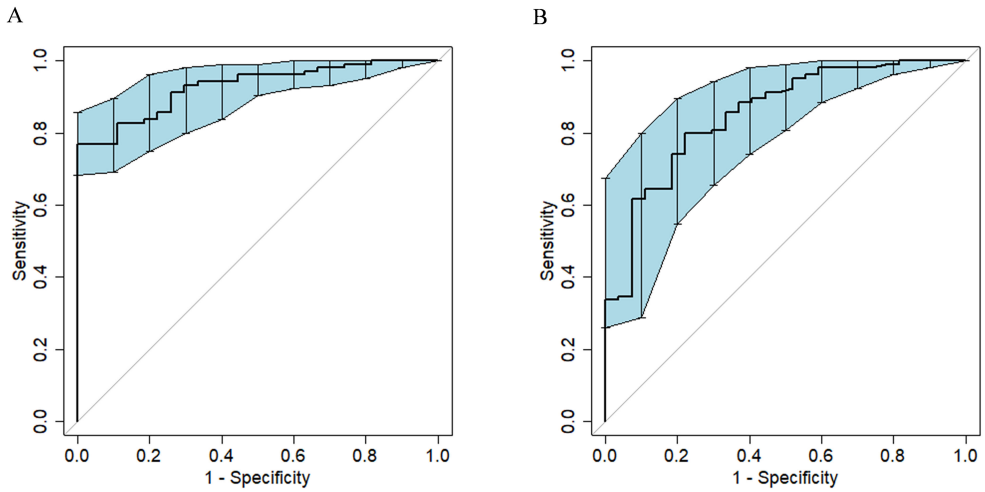


FIGURE 2
ROC curves of the model for predicting the efficacy of surufatinib in the treatment of HM-NENs. **(A)** Clinical–radiomics fusion model. **(B)** Radiomics model.

TABLE 3 Univariate and multivariate logistic regression analyses of the risk factors for the efficacy of HM-NENs.

| Variable | Univariable analysis | | Multivariable analysis | |
|---|---|---|---|---|
| | OR (95% CI) | *P*-value | OR (95% CI) | *P*-value |
| Radscore | 7.273 (3.431–18.94) | 0 | 8.808 (3.433–30.18) | 0.00s0* |
| Ki67 | 1.02 (1.006–1.036) | 0.008 | 1.035 (1.012–1.063) | 0.005* |
| Grade | 1.712 (1.138–2.667) | 0.012 | | |
| GGT | 1.004 (0.999–1.012) | 0.242 | | |
| AFP | 1.068 (1.009–1.18) | 0.114 | | |
| Diameter of the hepatic metastasis | 4.936 (1.724–21.01) | 0.01 | 4.050 (1.058–22.29) | 0.067 |
| Therapy method | 1.534 (0.95–2.508) | 0.082 | | |
| Surgery | 1.513 (0.606–4.16) | 0.394 | | |
| Number of hepatic metastases | 2.007 (1.051–4.059) | 0.042 | 3.795 (1.108–16.58) | 0.050* |
| NSE | 3.782 (1.425–9.941) | 0.007 | | |
| Extrahepatic metastasis | 5.75 (2.041–20.63) | 0.002 | 10.57 (2.137–79.68) | 0.009* |
| Sex | 0.898 (0.378–2.1) | 0.804 | | |
| Age | 1.003 (0.964–1.042) | 0.898 | | |
| Tumor location | 0.364 (0.149–0.858) | 0.022 | | |

HM-NENs, hepatic metastatic neuroendocrine neoplasms; NSE, neuron-specific enolase; Ki67, Ki67 antigen; AFP, alpha-fetoprotein; GGT, gamma-glutamyl transferase.
*$p < 0.05$.

center studies; single-center data may introduce selection bias, (2) the use of APCT images alone—integration with multiparametric MRI may improve accuracy, and (3) variations in scan parameters, reconstruction algorithms, and segmentation methods pose feature reproducibility challenges. While standardized techniques decreased these impacts, more preprocessing and feature extraction optimization are required. This study solely looked at the radiomics within the tumor and ignored the area surrounding it. In the future, the region of interest (ROI) around the tumor should be investigated to extract more radiomics properties.

Despite these limitations, this study demonstrated notable strengths. In the field of HM-NENs and surufatinib efficacy prediction, research employing clinical–radiomics models and visualized nomograms remained relatively scarce. This study

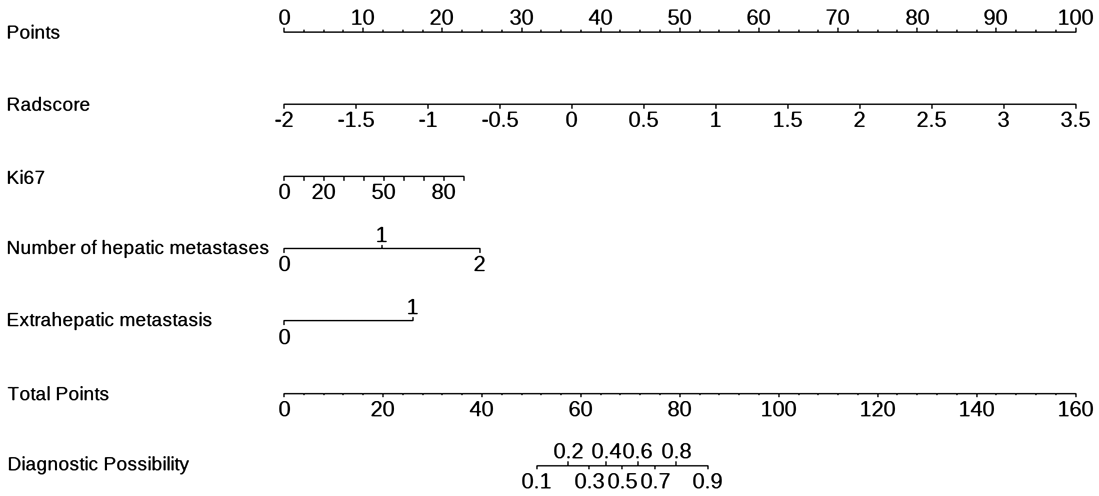


FIGURE 3
Nomogram for predicting the efficacy of surufatinib in HM-NENs.

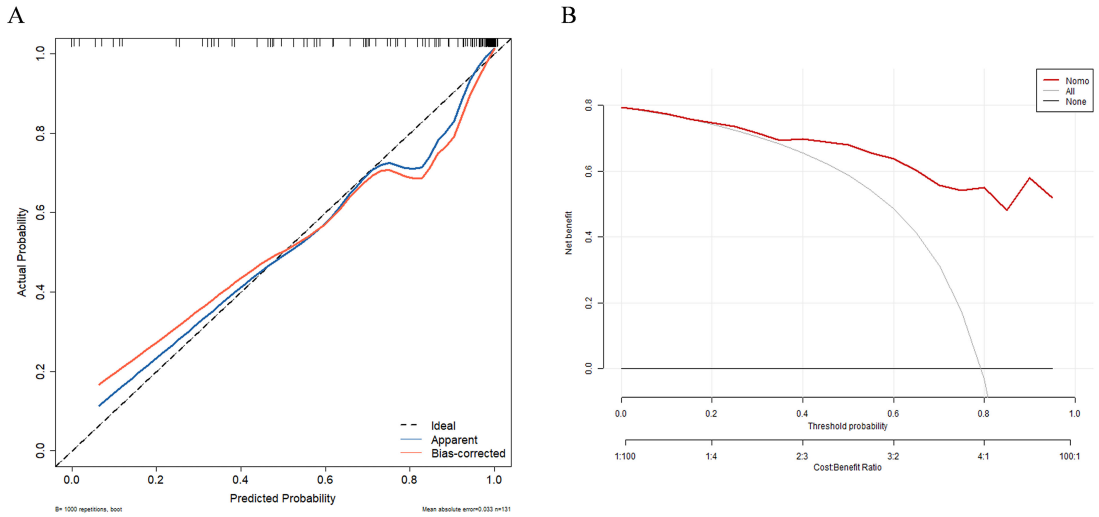


FIGURE 4
Calibration curve **(A)** and decision curve **(B)** of the clinical–radiomics fusion model. Calibration curves indicate the goodness-of-fit of the fusion model.

pioneered a novel exploratory pathway and established a foundation for subsequent multicenter, large-sample investigations. Radiomics technology enabled the extraction of radiomics features from CT images, and the models integrating clinical characteristics demonstrated effective predictive capabilities for surufatinib therapeutic response. The clinical–radiomics fusion models exhibited greater objectivity and comprehensiveness than traditional clinical evaluation methods. This advancement not only facilitated more informed clinical decision-making during treatment planning but also offered innovative perspectives and methodologies for personalized therapeutic strategies.

In conclusion, the APCT-based clinical–radiomics model with an AUC of 0.928 offered a noninvasive and visible analytical tool for the customized therapy of HM-NENs. Continued advances in radiomics technology promise to increase its role in precision medicine, eventually increasing treatment outcomes and survival rates.

## Data availability statement

The raw data supporting the conclusions of this article will be made available by the authors, without undue reservation.

## Ethics statement

The studies involving humans were approved by Fourth Hospital of Hebei Medical University. The studies were conducted in accordance with the local legislation and institutional requirements. Written informed consent for participation was not required from the participants or the participants' legal guardians/next of kin in accordance with the national legislation and institutional requirements.

## Author contributions

MF: Conceptualization, Data curation, Formal analysis, Investigation, Methodology, Software, Supervision, Validation, Visualization, Writing – original draft, Writing – review & editing. MZ: Supervision, Writing – review & editing, Conceptualization, Methodology. XD: Conceptualization, Supervision, Writing – review & editing, Formal analysis. JH: Conceptualization, Supervision, Writing – review & editing, Methodology. QW: Supervision, Writing – review & editing, Formal analysis, Project administration. FY: Formal analysis, Project administration, Supervision, Writing – review & editing, Funding acquisition, Resources.

## Funding

The author(s) declare financial support was received for the research and/or publication of this article. This work was supported by Wu Jieping Medical Foundation Scientific Research Special Grant Project: Study on Predicting the Efficacy of Surufatinib in Treating Liver Metastases from Neuroendocrine Neoplasms Based on Radiomics and Clinical Pathological Characteristics (Grant Number. 320.6750.2024 - 19-6); the S&T Program of Hebei, The Key Research And Development Plan Program of Hebei, the Health Innovation Program (Project Number: 22377788D, Project Name: Molecular typing and precise treatment of rectal neuroendocrine neoplasms); Local Science and Technology Development Fund of Hebei Province Guided by the Central Government of China through grant 246Z0102G. The funders had no role in the study design, data collection and analysis, decision to publish, or manuscript preparation.

## Acknowledgments

We thank and acknowledge all of the research staff from the Department of Gastroenterology at the Fourth Hospital of Hebei Medical University.

## Conflict of interest

The authors declare that the research was conducted in the absence of any commercial or financial relationships that could be construed as a potential conflict of interest.

## Generative AI statement

The author(s) declare that no Generative AI was used in the creation of this manuscript.

Any alternative text (alt text) provided alongside figures in this article has been generated by Frontiers with the support of artificial intelligence and reasonable efforts have been made to ensure accuracy, including review by the authors wherever possible. If you identify any issues, please contact us.

## Publisher's note



## Supplementary material

The Supplementary Material for this article can be found online at: https://www.frontiersin.org/articles/10.3389/fonc.2025.1628054/full#supplementary-material

## References

1. Chinese Society of Clinical Oncology Neuroendocrine Neoplasms Committee. Chinese consensus on gastroenteropancreatic neuroendocrine neoplasms (2022 edition). *Zhonghua Zhong Liu Za Zhi*. (2022) 44:1305–29. doi: 10.3760/cma.j.cn112152-20220812-00550

2. Hallet J, Law CH, Cukier M, Saskin R, Singh S. Exploring the rising incidence of neuroendocrine neoplasms: a population-based analysis of epidemiology, metastatic presentation, and outcomes. *Cancer*. (2015) 121:589–97. doi: 10.1002/cncr.29099

3. Pobłocki J, Jasińska A, Syrenicz A, Kozłowski K, Andrysiak-Mamos E. The neuroendocrine neoplasms of the digestive tract: diagnosis, treatment and nutrition. *Nutrients*. (2020) 12:1437. doi: 10.3390/nu12051437

4. Dasari A, Shen C, Halperin D, Zhao B, Zhou S. Trends in the incidence, prevalence, and survival outcomes in patients with neuroendocrine neoplasms in the United States. *JAMA Oncol*. (2017) 3:1335–42. doi: 10.1001/jamaoncol.2017.0589

5. Lauricella E, Manzoni B, Cavallo F, Milione M, Mazzaferro V. Angiogenesis in neuroendocrine neoplasms: biological mechanisms and therapeutic opportunities. *Front Oncol*. (2022) 12:957068. doi: 10.3389/fonc.2022.957068

6. Chinese Anti-Cancer Association Neuroendocrine Neoplasms Committee. Chinese guidelines for the diagnosis and treatment of neuroendocrine neoplasms (2025 edition). *Zhongguo Ai Zheng Za Zhi*. (2025) 35:85–142. doi: 10.19401/j.cnki.1007-3639.2025.01.010

7. Xu J, Shen L, Bai C, Li J, Wang J. Surufatinib in advanced pancreatic neuroendocrine tumours (SANEN-p): a randomised, double-blind, placebo-controlled, phase 3 study. *Lancet Oncol*. (2020) 21:1489–99. doi: 10.1016/S1470-2045(20)30493-9

8. Xu J, Shen L, Zhou Z, Li J, Wang J. Surufatinib in advanced extrapancreatic neuroendocrine tumours (SANEN-ep): a randomised, double-blind, placebo-

controlled, phase 3 study. *Lancet Oncol*. (2020) 21:1500–12. doi: 10.1016/S1470-2045(20)30496-4

9. Riihimäki M, Hemminki A, Sundquist K, Sundquist J, Hemminki K. The epidemiology of metastases in neuroendocrine tumors. *Int J Cancer*. (2016) 139:2679–86. doi: 10.1002/ijc.30400

10. Pavel M, Baudin E, Couvelard A, Krenning E, Öberg K. ENETS consensus guidelines for the management of patients with liver and other distant metastases from neuroendocrine neoplasms of foregut, midgut, hindgut, and unknown primary. *Neuroendocrinology*. (2012) 95:157–76. doi: 10.1159/000335597

11. Pavel M, O'Toole D, Costa F, Capdevila J, Gross D. ENETS consensus guidelines update for the management of distant metastatic disease of intestinal, pancreatic, bronchial neuroendocrine neoplasms (NEN) and NEN of unknown primary site. *Neuroendocrinology*. (2016) 103:172–85. doi: 10.1159/000443167

12. Frilling A, Modlin IM, Kidd M, Gustafsson B, Drozdov I. Recommendations for management of patients with neuroendocrine liver metastases. *Lancet Oncol*. (2014) 15:e8–e21. doi: 10.1016/S1470-2045(13)70362-0

13. Heneweer C, Holland JP, Divilov V, Carlin S, Lewis JS. Magnitude of enhanced permeability and retention effect in tumors with different phenotypes: 89Zr-albumin as a model system. *J Nucl Med*. (2011) 52:625–33. doi: 10.2967/jnumed.110.083998

14. Martínez-Jiménez F, Movasati A, Brunner SR, Priestley P, Van Hoeck A. Pan-cancer whole-genome comparison of primary and metastatic solid tumors. *Nature*. (2023) 618:333–41. doi: 10.1038/s41586-023-06054-z

15. Cappelli C, Boggi U, Mazzeo S, Campani D, Funel N. Contrast enhancement pattern on multidetector CT predicts Malignancy in pancreatic endocrine tumors. *Eur Radiol*. (2015) 25:751–9. doi: 10.1007/s00330-014-3485-2

16. Li S, Zhang P, Li J, Wang Y, Chen X. Radiomic signatures from MRI-based synovial vascularity mapping predict knee osteoarthritis progression. *Arthritis Rheumatol*. (2023) 76:1377–86. doi: 10.1002/art.42915

17. Zhang Y, Wang L, Chen X, Li H, Liu Y. Clinic-radiomics model using liver magnetic resonance imaging helps predict chronicity of drug-induced liver injury. *Hepatol Int*. (2023) 17:850–62. doi: 10.1007/s12072-023-10536-7

18. Zholdybay Z, Khusnutdinova G, Zhakenova Z, Tuleutayeva S, Alibek K. RECIST 1.1 and mRECIST 1.1: radiological assessment of tumor response to chemotherapy (literature review). *Vestn KazNMU*. (2021) 3):291–5. doi: 10.53065/kaznmu.2021.35.60.056

19. Song J, Yin Y, Wang H, Chang Z, Liu Z. A review of original articles published in the emerging field of radiomics. *Eur J Radiol*. (2020) 127:108991. doi: 10.1016/j.ejrad.2020.108991

20. Kostanek J, Karolczak K, Kuliczkowski W. Bootstrap method as a tool for analyzing data with atypical distributions deviating from parametric assumptions: critique and effectiveness evaluation data (Basel). *Data*. (2024) 9:95. doi: 10.3390/data9080095

21. Francis A, Venkatesh GH, Zaarour RF, Hassan M, Azizi F. Tumor hypoxia: a key determinant of microenvironment hostility and a major checkpoint during the antitumor response. *Crit Rev Immunol*. (2018) 38:505–24. doi: 10.1615/CritRevImmunol.2019030168

22. Dercle L, Lu L, Schwartz LH, Frasure SE, Fojo AT. Radiomics response signature for identification of metastatic colorectal cancer sensitive to therapies targeting EGFR pathway. *J Natl Cancer Inst*. (2020) 112:902–12. doi: 10.1093/jnci/djaa017

23. Lambin P, Leijenaar RTH, Deist TM, Peerlings J, Gillies RJ. Radiomics: the bridge between medical imaging and personalized medicine. *Nat Rev Clin Oncol*. (2017) 14:749–62. doi: 10.1038/nrclinonc.2017.141

24. Miszczuk M, Chapiro J, Do Minh D, Savic LJ, Lin M. Analysis of tumor burden as a biomarker for patient survival with neuroendocrine tumor liver metastases undergoing intra-arterial therapies: a single-center retrospective analysis. *Cardiovasc Intervent Radiol*. (2022) 45:1494–502. doi: 10.1007/s00270-022-03209-9

25. Sun J, Xia D, Bai W, Li X, Wang L. Tumor burden affects the progression pattern on the prognosis in patients treated with sorafenib. *Front Oncol*. (2024) 14:1405178. doi: 10.3389/fonc.2024.1405178

26. Wang W, Zheng H, Jiang J, Li D, Zhang Y. Engineering micro oxygen factories to slow tumor progression via hyperoxic microenvironments. *Nat Commun*. (2022) 13:4495. doi: 10.1038/s41467-022-32066-w

27. Gillies RJ, Kinahan PE, Hricak H, Schöder H, Weber WA. Radiomics: images are more than pictures, they are data. *Radiology*. (2016) 278:563–77. doi: 10.1148/radiol.2015151169

28. Zhang Y, Tan Y, Yuan J, Tang H, Zhang H, Tang Y, et al. circLIFR-007 reduces liver metastasis via promoting hnRNPA1 nuclear export and YAP phosphorylation in breast cancer. *Cancer Lett*. (2024) 592:216907. doi: 10.1016/j.canlet.2024.216907

29. Zeng Y, Du W, Huang Z, Wu S, Ou X, Zhang J, et al. Hsa_circ_0060467 promotes breast cancer liver metastasis by complexing with eIF4A3 and sponging miR-1205. *Cell Death Discov*. (2023) 9:153. doi: 10.1038/s41420-023-01448-4